

MEMS MIRROR BASED EYE TRACKING: SIMULATION OF THE SYSTEM PARAMETER EFFECT ON THE ACCURACY OF PUPIL POSITION ESTIMATION

Mateusz Pomianek, Marek Piszczek, Marcin Maciejewski

Military University of Technology, Institute of Optoelectronics, 2 Kaliskiego St., 00-908 Warsaw, Poland
(✉ mateusz.pomianek@wat.edu.pl, +48 261 839 627, marek.piszczek@wat.edu.pl, marcin.maciejewski@wat.edu.pl)

Abstract

Eye tracking systems are mostly video-based methods which require significant computation to achieve good accuracy. An alternative method with comparable accuracy but less computational expense is 2D microelectromechanical (MEMS) mirror scanning. However, this technology is relatively new and there are not many publications on it. The purpose of this study was to examine how individual parameters of system components can affect the accuracy of pupil position estimation. The study was conducted based on a virtual simulator. It was shown that the optimal detector field of view (FOV) depends on the frequency ratio of the MEMS mirror axis. For a value of 1:13, the smallest errors were at 0.1° , 1.65° , 2.3° , and 2.95° . The error for the impact of the signal sampling rate above 3 kHz stabilizes at 0.065° and no longer changes its value regardless of increasing the number of samples. The error for the frequency ratio of the MEMS mirror axis increases linearly in the range of 0.065° – 0.1° up to the ratio of 1:230. Above this there is a sudden increase to the average value of 0.3° . The conducted research provides guidance in the selection of parameters for the construction of eye tracking MEMS mirror-based systems.

Keywords: eye tracking, MEMS mirror, laser scanning, head-mounted display.

© 2021 Polish Academy of Sciences. All rights reserved

1. Introduction

Eye tracking systems are being used more and more frequently for various tests in medicine, psychology, computer systems, automotive industry and market analysis [1–3]. They allow to track eyeball movements in terms of analysis of incorrect eye movement or determination of the user's fixation point [4]. In the first case, such analysis can allow for diagnosis of a range of neurological diseases [5, 6]. The determination of a point observed by the user is applied in practical analyses of concentration and as interfaces of communication with the device. Eye tracking systems have also become available in consumer solutions for work or entertainment. One of such solutions are *virtual reality* (VR) technologies. They generate a virtual space which is observed by the user through a dedicated device (*head-mounted display* – HMD). It collects

simultaneously the information on the orientation, position (depending on the model) and activities carried out by the user. Based on such information, the computer system updates the virtual environment and the image transmitted to the user. The application of the eye tracking system in this technology allows for the direct determination of a fixation point in the 3D space as well as generating the environment's response to its change. Such solutions allow for simple construction of communication interfaces with the virtual environment and also the control and analysis of the user's behaviour, which has not been possible so far [7, 8]. The HMD for virtual reality systems is more often produced as independent wireless systems. Becoming independent from wires and an external computing machine allows for comfortable work and reduces the costs of the device itself. Nevertheless, eye tracking systems in virtual technologies are currently available only as part of the HMD connected with the stationary computing unit. This results from analytical complexity of the solutions applied which cannot be managed by an independent mobile device.

Today's eye tracking systems are based mostly on methods of optical analysis using radiation reflected from eyeballs. The vast majority of these systems are video-based ones (the video-based method). This is the most common method on account of its non-invasiveness and a low price. The image is intercepted by means of a video camera and eye movement is determined based on the difference in the dislocation of marker edges (characteristic curves) in subsequent images (usually they are based on the so-called Purkinje's imaging) [9]. Along the technological development, traditional vision cameras have been replaced with those operating in the *infrared* (IR) range. This enabled the illumination of the image with the radiation invisible to the user, reduction of interferences and improvement of eye tracking quality. This method is based on image analysis applied in order to determine the accurate pupil position. Its accuracy depends directly on the video camera resolution and its operation rate (movements which it is able to detect). Nevertheless, increasing the video camera resolution raises exponentially the number of calculations which are necessary during image processing. The operation rate of the video cameras available is also limited by the technology which is accessible and the possibilities of data transfer. Consequently, eye tracking in this technology with satisfactory accuracy is connected with the necessity of conducting lots of computations within a single video camera frame. Enhancing the operation rate reduces the time for carrying out these operations even more. This prevents using this technology in mobile HMD systems. Therefore, there are tests being performed on eye tracking systems which do not require such a high number of computations [10–12].

One of alternative optical detection methods using the signal reflected from the eyeball is MEMS – mirror scanning method [13–16]. These systems work based on MEMS movable mirrors scanning the area of the eyeball along a specific curve. The analysis of a single data vector does not require high computational capabilities and it can be performed on a micro-controller. The operation rate of such systems can be even several dozen times higher than in the case of systems which are based on video cameras (3.5 kHz instead of 90 fps). This is important because it gives the ability to detect, sample (at least 10 measurements) and accurately analyse more types of eye movements (*e.g.* smooth pursuit – 50–150 Hz, or saccades – over 200 Hz). This method also seems to be proper for application in HMD mobile devices, solving the problems of low computational capabilities of such devices. Due to previous unavailability of element miniaturisation, such solutions have not been tested well and they are not described in the literature. Therefore, it is necessary to conduct more detailed analyses of this method. Our research is based on the concept initially presented in the literature. However, there are no publications containing information on the accuracy of such methods or of impact of individual parameters on the functioning of such a system. This paper presents tests conducted in terms of impact of the eye tracking system parameters by means of the MEMS

mirror scanning method on the pupil position estimation errors. The initial tests were published in the post-conference materials of the MicDAT[®] 2020 Conference [17]. The scope of the topic is shared, but the study was completely redone with an expanded scope (the measurement tool has been rebuilt and improved, with new measurements taken at better resolution and over a wider range).

2. Materials and methods

The tested eye tracking method was based on the MEMS mirror movement. The model of the mirror operating on two axes in the resonance mode had been assumed. On account of the fact that one axis operates usually with a frequency higher than the other, there is the division into the fast axis and the slow axis. A curve drawn on the eye surface by the normal vector to the mirror, during such a type of motion, is described with Lissajous figures in accordance with equations presented below:

$$\begin{aligned} x(t) &= A \cdot \sin(at + \delta), \\ y(t) &= B \cdot \sin(bt). \end{aligned} \quad (1)$$

The method under discussion collects samples synchronously with the mirror motion. During the mirror movement the data are collected in the buffer and transmitted for analysis after collecting the full series constituting a single period of the slow axis movement. Hence, the implementation time depends directly on the operation frequency of the MEMS mirror slow axis. Since the mirror is located beyond the eye axis, detection is carried out by means of the dark pupil technique. The light reaches the eye surface and it is subject to dispersion. The sensor registers the intensity of reflected radiation. This, in turn, differs depending on the type of beam dispersion surface. Passing through the pupil area during scanning is characteristic for the signal drop (darker area), and going beyond this area is characteristic for the increase in the signal intensity. Pupil position is determined based on the local intensity extremes. The point image position is determined based on the comparison to the curve model formed on the basis of information on axis frequencies. The determined points of the pupil area intersection are described with an ellipse through matching by means of the least squares method. The ellipse midpoint estimates to the eye pupil centre. A further analysis in terms of determining the eyesight direction and fixation point is analogous to the video-based method. Fig. 1 provided below, presents the algorithms of the acquisition and analysis of the method under discussion.

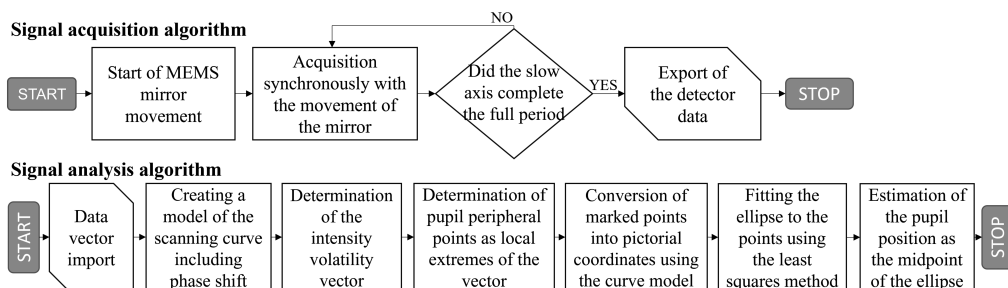


Fig. 1. Algorithms of signal acquisition and processing in the eye tracking system based on scanning the eye area with the MEMS 2D mirror.

The main benefit of eye tracking by means of the MEMS scanning method, as compared to the video camera image analysis, is lower number of computations necessary for determining the pupil position. Therefore, the eye tracking system in these tests was adjusted to mobile solutions. The target configuration anticipated installation in the HMD type device. This system is significant due to the point of locating the MEMS mirror. It is located beyond the lens area in order not to cover the user's field of view in the target HMD device. The eye is scanned in the NIR (*near infrared*) range, making it invisible to the user. Moreover, an image displayed in HMD does not affect the signal within this range. As far as the eye tracking system is concerned, the lighting system, as well as the detection system, follow the same optical path. They both pass through the MEMS mirror. When changing its displacement in two axes, it scans the eye area. One mm was assumed as the MEMS mirror diameter. However, depending on the inclination of the mirror, its position and orientation of the eyeball, the size of the illuminated area changes. Therefore, the field of view in degrees (from the point of view of the MEMS mirror) was assumed as the dependent variable. The boundary condition for the beam discrepancy was the diameter of the MEMS mirror (1 mm) through which it passes and expressed as a field of view. The focal plane was the centre of the pupil in the direction of the eye looking straight ahead. The operation of the system was verified in OSLO optical simulation software (version 20.2). The measurement system diagram is presented in Fig. 2.

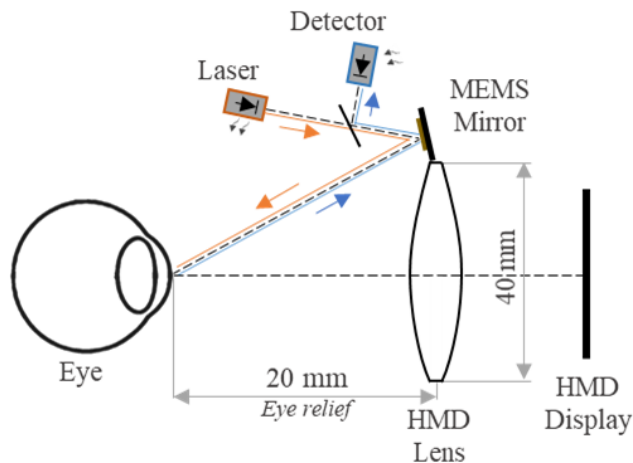


Fig. 2. Spatial distribution of the system elements.

The measurement system with the components described was modelled in the Unity environment (version 2019.4.14f1). This tool allows for simulation and 3D visualization of spaces and objects. During work, it takes into account the geometric relationships between objects and the basic physical phenomena. The Unity environment is also used for scientific purposes related i.a. to real-time simulations [18–20]. Three main object groups were implemented: a face and eyes, the HMD and the eye tracking system elements. The operation algorithms were designed for each of the elements formed. This allowed to simulate the co-operation of the set of elements in virtual space. An eyeball as a 3D model constitutes a single block. Consequently, the effects of the light penetrating inside the eye were simulated through change in the reflectiveness of the pupil surface (maximum absorption). Nevertheless, its cornea has reflectiveness and transparency similar to the real one.

The simulator consists of modules implementing respective functions – simulations, the spatial configuration of elements, image acquisition, conducting measurements, data export. The software is capable of simulating the light only in the visual spectrum. Hence, the overall preview of the eye area is darkened (all the light sources are deactivated) during the measurement. The only source left is the light from the illuminator. A virtual video camera fulfils the role of a detector whose visual area is summed up as a single value of intensity. The resolution of the virtual video camera is 64×64 pixels, and its field of view is set at the beginning of the measurement. Such a solution allows to consider and compensate perspective changes during the movement and the occurring distortions. On account of the modular structure of the simulator, it is possible to modify the series of the parameters and the settings of the system elements. In the virtual user's group, it is possible to modify: eye span, eye colour, pupil size and iris size. Furthermore, the fixation point position is also set in the virtual space (eyeball orientation). It is limited in this software to the HMD field of view. In the case of the eye tracking elements of the system, the following is modifiable: a scanning curve type (the ratio of the MEMS mirror axis), a mirror displacement range, the detector field of view, an illuminator spot size. Moreover, the quantity of samples during scanning is limited by the software. The spatial configuration of the system of elements is also changeable. This enables conducting tests in terms of impact of the MEMS mirror position in the HMD on the accuracy of pupil position determination.

The output element of the measurements in the virtual environment are vector data, image data and metadata carrying information on the type and the spatial system of the elements during the measurement. The intensity vector and additional metadata are transferred in the JSON format. The matrix of the eye area image seen from the perspective of the MEMS mirror, which serves as a basis for data analysis, is also included in the file. The data analysis module, on account of its operational rate, was implemented in the MATLAB environment (version R2020b). The accuracy of simulation data with reference to real image signal was verified based on real image data from the commercial device Pupil Core of Pupil Labs company. The 3D model of the simulation environment was built based on real images from the Pupil Labs device. The iterative method was used to introduce corrections so that the difference between the two was as small as possible. When the appropriate level of reproduction of the real scene was achieved, it became possible to carry out measurements based on the calibrated virtual environment. An example of the data analysis from the prepared simulator compared to the model data is presented in Fig. 3.

Based on the prepared simulator, the tests of the impact of the main parameters of the eye tracking system elements (the detector field of view, a signal sampling frequency, the ratio of the MEMS mirror axis frequency) on pupil position estimation accuracy were carried out. The detector *field of view* (FOV) is not understood as the total scanning area, but as the temporal (moving) observed region. This is due to the design of the optical system. The detector “looks through” the scanning MEMS mirror and its FOV depends directly on the selected lens power. Furthermore, the accuracy of the MEMS mirror scanning method was verified for spatial distribution of the system elements in the HMD. For each tested dependence, two to six independent sessions were conducted in various spatial configurations. Measurements were made for eyes during fixation set on a specific point. Additional image effects such as PSF and corneal reflection were determined, accounted for, and eliminated during analysis in the MATLAB environment. All the measurements are statistically significant with the significance level $\alpha = 0.005$ on the basis of verification of significance of the correlation coefficient by means of the non-parametric test.

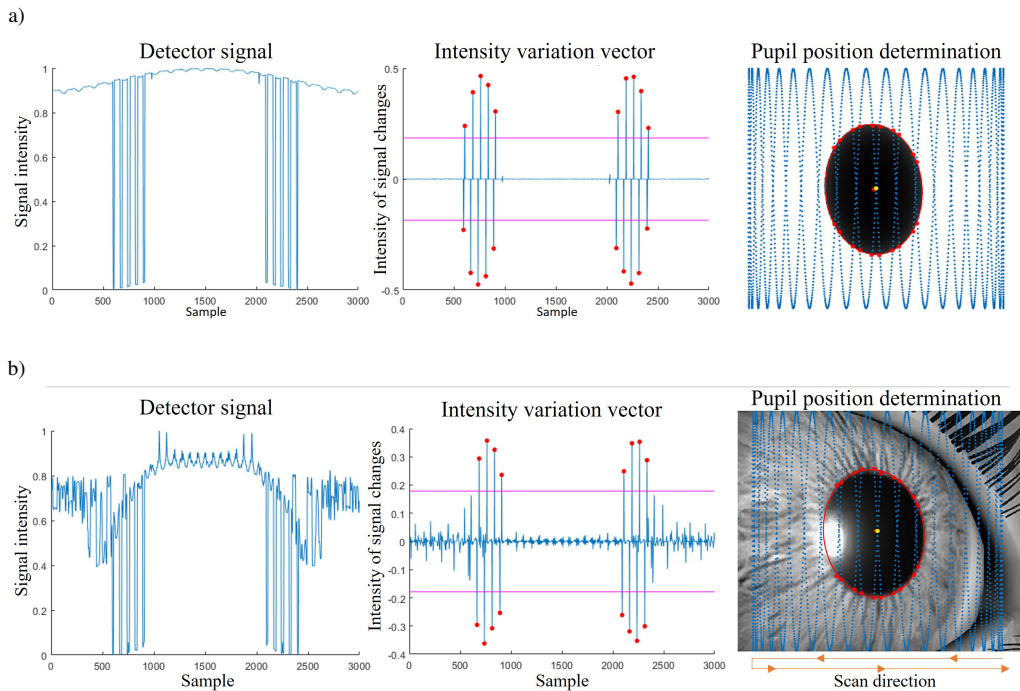


Fig. 3. Pupil position determination: a) on the model image, b) on the simulation data.

3. Results

3.1. The impact of spatial configuration of the system elements

Based on the developed simulator, in-silico tests were carried out concerning the impact of spatial configuration on pupil estimation error. The analysis involved the position variation of the MEMS mirror in the HMD system. Because of the spatial arrangement of the device, the MEMS mirror (as a signal source) was shifted along the HMD lens perimeter (right). The position was changed every 7.5° , starting from the clockwise upper setting. The total number of the checked configurations amounted to 48. Regardless of its position, the mirror maintained the horizontal position of the slow axis and the vertical position of the fast axis. The series of measurements were analysed for the ratios of the MEMS mirror axis frequencies equalling 15, 20, 25 and 30 at the eyeball fixation of 15 cm (correlation 0.98, SD = 0.12°) and for infinity (correlation 0.88, SD = 0.02°). The measurements were carried out for the sampling frequency of 4 kHz, the detector field of view of 0.2° , the displacement of the MEMS mirror axis of $\pm 10^\circ$ and the pupil size of 5 mm. For fixation in infinity, the largest error (0.12° , SD 0.02°) was present in the position of 45° , and the smallest one (0.03° , SD 0.01°) at 232.5° . For fixation in 15 cm, the largest error (1.07° , SD 0.18°) was present in the position of 52.5° , and the smallest one (0.09° , SD 0.02°) at 330° .

The data were averaged to the form of a single curve. An average error was 0.294° . Three positions may be differentiated on the curve, where the error has a low value. The first of them occurs at the angle of 180° , where the error is 0.114° (a drop by 61% in relation to the mean). The

second minimum occurs at 277.5° , and the error is 0.068° (a drop by 77%). The third minimum occurs at 337.5° , and the error is 0.086° (a drop by 71%). The largest error occurs at the angle of 52.5° , where the error is 0.59° (an increase of 101% in relation to the mean). The results together with the diagram of the positions are presented in Fig. 4.

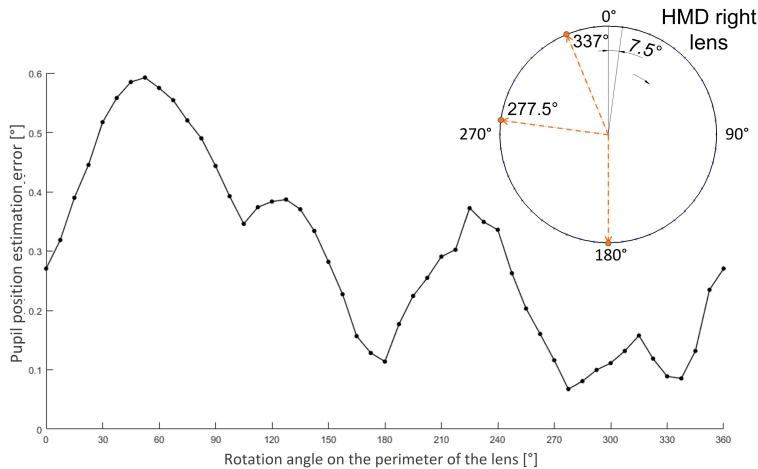


Fig. 4. The impact of the averaged MEMS mirror position signal on the lens perimeter on the pupil position estimation error.

3.2. The impact of parameters of the system element

The tests of the detector FOV demonstrated that as its value increased, the pupil position estimation error fluctuated at specific intervals. The measurements were conducted for 2 spatial configurations in the range of the field of view of 0.05° – 3° with a step of 0.05° . Each series was analysed in three variants with the various detection thresholds of signal variation intensity (a criterion of qualifying a curve point as the pupil intersection). The respective thresholds were as follows: 0.2, 0.35, 0.5 of the signal variation derivative value. The average standard deflection in the averaged measurement point was $SD = 0.019^\circ$. The correlation coefficient between the curves was on average 0.60 ($SD = 0.21$). The signal variation range in the curve obtained was 0.056° , at the maximum value of 0.11° ($SD = 0.014^\circ$). The signal had local maximums for the approximate value of 0.5° , 1.1° , 1.85° and 2.85° . These values repeated in each series. The tests were conducted at the displacement range of the MEMS mirror axis of $\pm 10^\circ$, their frequency ratio of 13 and the sampling frequency of 4 kHz. The measurements were carried out for the fixed eye pupil of 5 mm. This value resulted in 14° of mirror displacement. The graph of the impact of the detector field of view on the pupil position estimation error is presented in Fig. 5.

As the detector field of view increased, the number of the determined pupil intersection points increased as well. For detector FOV $< 1^\circ$, this growth equals on average 11.5 ($SD = 1$) (24–35 points). Above this value, it slows down to the value of 2.25/ 1° ($SD = 1.04$) and it stabilises at the level of 42. The actual value of the pupil area intersection with the scanning curve for a single period of the slow axis of the mirror was 24. Additional detected points are from lines located beyond the pupil area; nevertheless, on account of the wide field of view, they are detected.

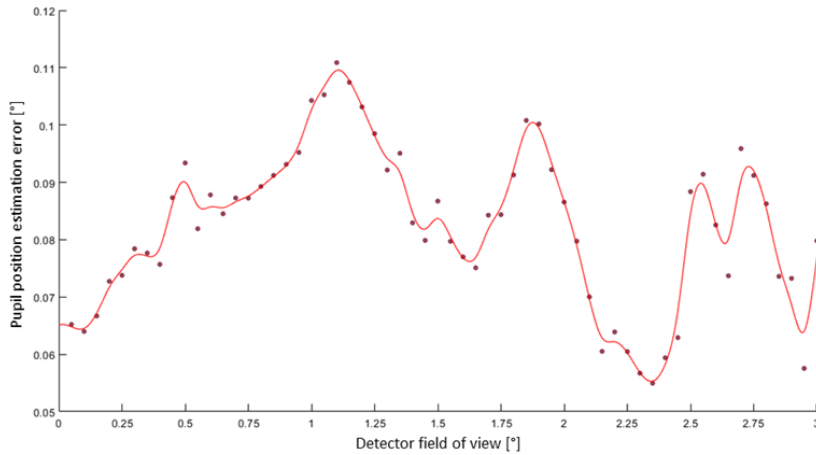


Fig. 5. Graph of the impact of the detector field of view on the pupil position estimation error.

As the detector field of view increased, the area from which an averaged signal was collected, grew as well. It means that the FOV increase was connected with the decrease in the signal variation intensity (due to averaging). For the variation of 0.05° – 3° , the maximum signal derivative value dropped by 0.62 (0.72–0.1). The graph of the variation of the maximum signal derivative is presented in Fig. 6 below.

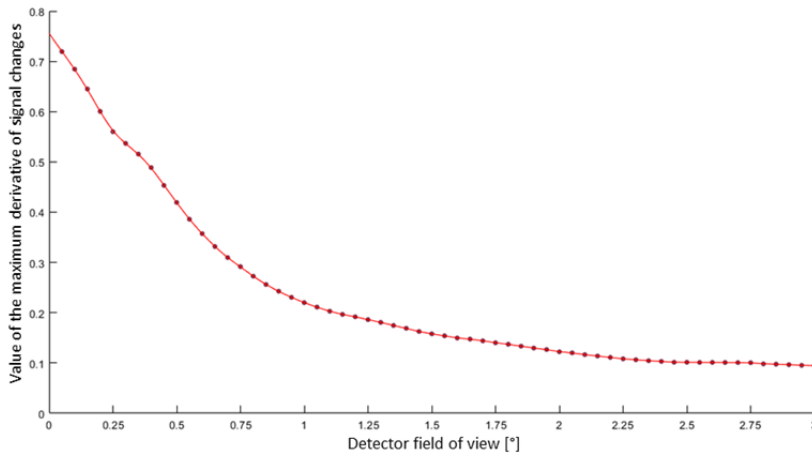


Fig. 6. Graph of the detector field of view impact on the signal derivative value variation.

The sampling frequency tests demonstrated that the increase in the sample quantity was interrelated with the decrease of the pupil position estimation error. Below 1 kHz, the error rate was as high as 0.3° . As the frequency increased, the error was aiming for a stable value of about 0.065° . The measurements were carried out in the following range 200 Hz:10 kHz with a step of 10 Hz. The tests were conducted at the displacement range of the MEMS mirror axis of $\pm 10^\circ$ and its frequency ratio of 13. The detector field of view was 0.1° . Three series of data were performed for various mirror spatial configurations. The correlation coefficient between subsequent series

was 0.7, and the average standard deflection between their samples amounted to 0.008° . The pupil point detection threshold was 0.4 of the maximum derivative value. The graph of the impact of the signal sampling frequency on the pupil position estimation error is presented in Fig. 7.

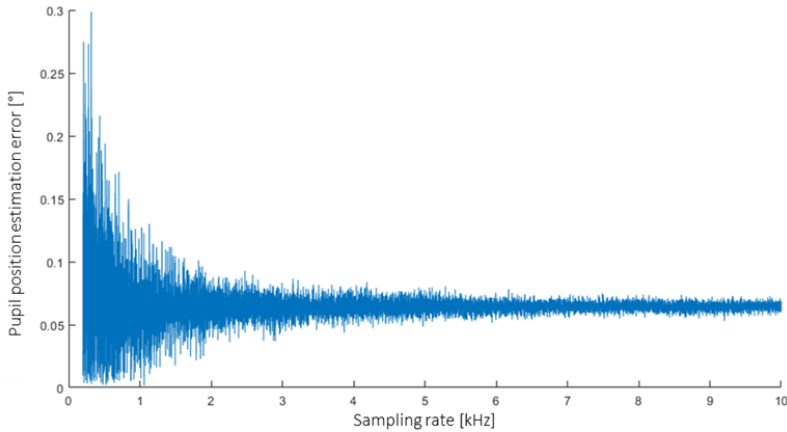


Fig. 7. Graph of the signal sampling frequency impact on the pupil position estimation error.

The error value for respective values of the signal sampling frequency was fluctuating. An average error was 0.065° . The standard deviation in the range below 2 kHz amounted to 0.048° (max 0.17°); whereas, above this value, it was on average 0.002° . Therefore, the curve standard deviation analysis was conducted in the sampling frequency increase function. Standard deviation was measured for the batch of 10 samples on the surface of the full measurement range. The results are presented in Fig. 8.

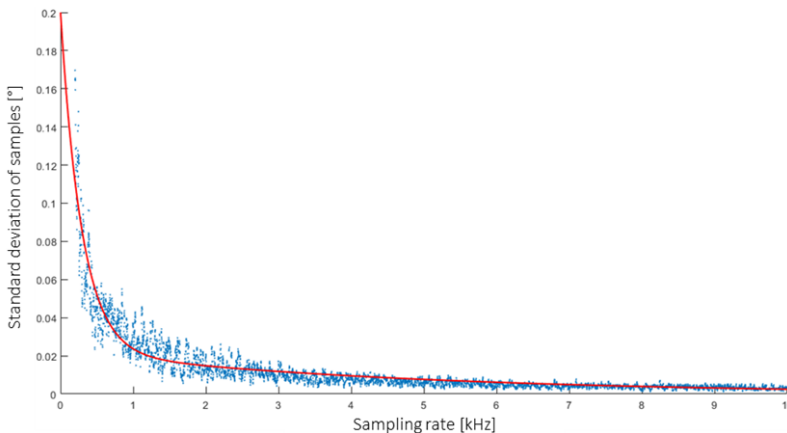


Fig. 8. Graph of the standard deviation of errors in the sampling frequency function.

The tests on the ratio of the mirror axis frequency showed that its growth is interrelated with the increase in the pupil position estimation error. By mirror axis frequency ratio is meant the frequency of the slow axis control signal divided by the frequency of the fast axis control signal. Three series of measurements were performed which differed in spatial configurations. Each of

them included 346 measurement samples within the axis frequency ratio of 5–350. The correlation coefficient between subsequent series was 0.75, and the standard deviation of the averaged sample amounted to 0.063° . The measurements were conducted for the sampling frequency of 4 kHz and the detector field of view of 0.1° . In the range of the axis frequency ratio of 5–230, the error on average was 0.072° ($SD = 0.002$), and its growth was 0.113° (0.05–0.16). Whereas, in the range of 230–350, the average error amounted to 0.26° ($SD = 0.11^\circ$), and the growth was at the level of 0.45° (0.15–0.60). The results are presented in Fig. 9.

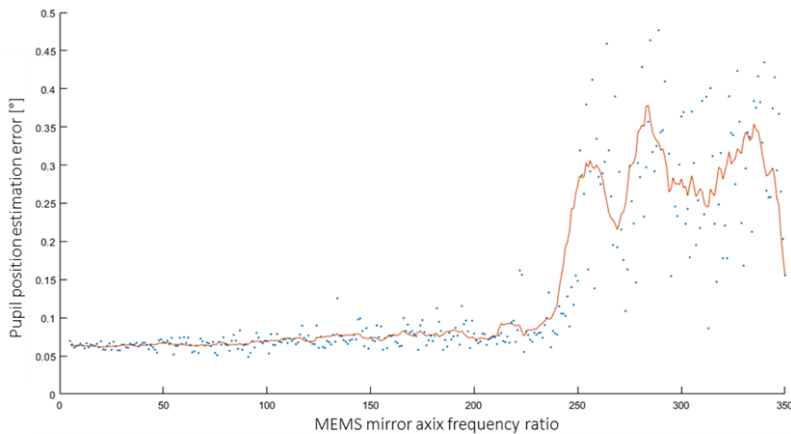


Fig. 9. Impact of MEMS mirror frequency ratio on the pupil position estimation error.

4. Discussion

The analysis of the VR simulator virtual data has indicated that there is the perpendicular signal reflection from the eyeball (it is simulated). In such a situation, there is abrupt growth in signal intensity, which introduces erroneous detection of the pupil intersection point. Due to the fact that this intensity growth occurs above the average value of the signal reflected from the sclera (the pupil area intersection is located below), its detection and elimination is possible. The impact of this signal also decreases as the intensity of the signal emitted by the illuminator grows. In the future, it is planned to determine (based on physical measurements) the dependence between the simulated virtual intensity and the physical values of the illuminator in Watts. The use of laser power will also entail safety considerations so as not to cause negative biological effects on the user.

The tests concerning the impact of the spatial arrangement of the eye tracking elements demonstrated that, depending on the position, the pupil position estimation error may change its value even 8 times. Although the eyeball seems to be symmetrical, the research also took into account the surrounding face. Therefore, the results were also influenced by the eyelashes, eyelids and nose. Depending on the position of the mirror, the relative share of these elements in the observed image changed. Especially eyelashes were sometimes determined as the point of intersection of the pupil and caused false positive errors. On the basis of the tests carried out, three positions were allocated at which the estimation error is minimal. These are possibly the best places to locate the MEMS mirror in the physical system. On account of the HMD structure and a nose notch, the best position seems to be at the angle of 180° or 337.5° (rotation in relation to the upper position). Furthermore, the tests demonstrated that in the frequently used position of

90° (location at the right-hand side of the right lens), despite the slight drop in the error, it is still 15% larger than the average value of all the positions. The correct selection of the MEMS mirror allows for error reduction by even 77% in relation to the average error.

The tests performed on the detector field of view showed that the signal fluctuates at specific time intervals. They result from the dependences between the distances between the scanning curves and the diameter of the area observed on the eye surface. As the detector field of view increases (or the concentration of the scanning line), the number of the detected pupil perimeter points grows as well. However, when the detected new points are not symmetrical, it shifts the detected pupil centre towards the said additional points, at the same time increasing the error. When the detector FOV is increased further, the symmetrical points on the opposite side of the pupil are also detected and the error decreases. The intervals of the periodical error growth result from the periodical increase in additionally detected pupil perimeter points. Increasing the detector field of view also increases the area from which the signal is averaged. It reduces the intensity of signal variation, while smoothing its slopes. This is crucial in terms of signal analysis. If the field of view is small, passing through the pupil area takes place only between two points. Yet, if it occurs on the surface of a few points, it is critical to determine in relation to which of them the pupil perimeter point is defined. Lower signal intensity may result in a failure to detect some passages through the pupil area. Nevertheless, a larger averaging area reduces random errors occurring for the low detector FOV ($< 0.2^\circ$), at the same time decreasing the pupil position estimation error. By decreasing the detector field of view such random errors can be eliminated, *e.g.* through averaging the signal from a few measurements in a single scanning point.

The signal sampling frequency determines the number of detection samples which is collected during a single period of the MEMS mirror slow axis. The parameter is similar to resolution in visual systems. The tests proved that as the sampling frequency rises, the pupil position estimation error decreases to a certain level. Below approximately 1 kHz, the error ranges $0\text{--}0.3^\circ$. Above this area, it aims at stabilisation at the level of approximately 0.065° . Measurement fluctuations arise from different distribution of measurement points in the scanning curve with reference to the fixed pupil position during measurements. Moreover, the standard deviation of samples also decreases along with the increase in the sampling frequency from the value of 0.2° to 0.005° . Higher number of samples increases the accuracy of the pupil position determining. At the same time, it also increases the number of necessary computational operations. As far as mobile systems are concerned, computational conservation is of particular importance. At the same time, the accuracy gain is not linear but it stabilises at a constant value. Thus, the optimal signal sampling range in terms of its use in mobile systems is 2–4 kHz. The signal sampling frequency should also be selected with consideration of the ratio of the mirror axis frequency.

The frequency ratio of the MEMS mirror axis is seen directly in the shape of the eyeball scanning curve. Low values indicate lower number of fast axis scans as compared to the slow axis. At the same time, the lower this number is, the closer to each other are distributed the measurement points on the curve. This increases the measurement accuracy but it also increases the standard deviation of the results. This is caused by the occurrence of “dead fields” in which too few scanning lines pass through the pupil in order to determine its position accurately. The tests of the ratio of the axis frequency showed that its growth is interrelated with the increase in the pupil position estimation error. Up to the value of approximately 230, this error grows slowly in the range $0.06^\circ\text{--}0.1^\circ$. Above this value, there is sudden growth and the error increases on average by 76% to the value of 0.3° and it fluctuates in the range $0.1^\circ\text{--}0.5^\circ$. At the same time, the standard deviation within the axis frequency ratio also grows significantly to 250–350. The tests performed prove that the applied analysis algorithm cannot be used to effectively define the pupil

position above the limit value of the MEMS mirror frequency ratio which is 230. For mirrors operating in this range, it may be necessary to re-build the algorithm. In practical implementation, it will also be necessary to take into account the MEMS mirror control method. The deflection of the mirror most often depends on the given voltage, the range of which will have to be operated by the mobile device.

5. Conclusions

The prepared simulator enabled the determination of curves of dependences between key parameters of the eye tracking system based on the MEMS mirror motion. On the basis of the tests conducted, their optimal values were determined. The simulations performed allow for preparing a physical test stand with parameters minimising the pupil position estimation error which results from them. The construction of such a stand type enable further tests of the eye tracking system based on the MEMS mirror. At the same time, the tests carried out acknowledged the usefulness of virtual space simulators in the range exceeding the possibilities of the numerical analysis based on the written code. Furthermore, it is planned to conduct the analyses of other new algorithms of data processing in the eye tracking systems by means of the MEMS mirror method.

Acknowledgements

The research was funded by the Military University of Technology, Grant Number ZBW/08-893/2020/WAT and Remmed VR.

References

- [1] Duchowski, A. T., (2017). *Eye tracking methodology: Theory and practice*. Springer. <https://doi.org/10.1007/978-3-319-57883-5>
- [2] Judd, T., Ehinger, K., Durand, F., & Torralba, A. (2009, September). Learning to predict where humans look. *IEEE 12th International Conference on Computer Vision* (pp. 2106–2113). IEEE. <https://doi.org/10.1109/ICCV.2009.5459462>
- [3] Goldberg, J. H., & Kotval, X. P. (1999). Computer interface evaluation using eye movements: methods and constructs. *International Journal of Industrial Ergonomics*, 24(6), 631–645. [https://doi.org/10.1016/S0169-8141\(98\)00068-7](https://doi.org/10.1016/S0169-8141(98)00068-7)
- [4] Hansen, D. W., & Ji, Q. (2009). In the eye of the beholder: A survey of models for eyes and gaze. *IEEE Transactions on Pattern Analysis and Machine Intelligence*, 32(3), 478–500. <https://doi.org/10.1109/TPAMI.2009.30>
- [5] Carvalho, N., Laurent, E., Noiret, N., Chopard, G., Haffen, E., Bennabi, D., & Vandel, P. (2015). Eye movement in unipolar and bipolar depression: A systematic review of the literature. *Frontiers in Psychology*, 6, 1809. <https://doi.org/10.3389/fpsyg.2015.01809>
- [6] Bittencourt, J., Velasques, B., Teixeira, S., Basile, L. F., Salles, J. I., Nardi, A. E., Budde, H., Cagy, M., Piedade, R., & Ribeiro, P. (2013). Saccadic eye movement applications for psychiatric disorders. *Neuropsychiatric Disease and Treatment*, 9, 1393. <https://doi.org/10.2147/NDT.S45931>
- [7] Duchowski, A. T., Medlin, E., Gramopadhye, A., Melloy, B., & Nair, S. (2001, November). Binocular eye tracking in VR for visual inspection training. *Proceedings of the ACM symposium on Virtual reality software and technology* (pp. 1–8). <https://doi.org/10.1145/505008.505010>

- [8] Blattgerste, J., Renner, P., & Pfeiffer, T. (2018, June). Advantages of eye-gaze over head-gaze-based selection in virtual and augmented reality under varying field of views. *Proceedings of the Workshop on Communication by Gaze Interaction* (pp. 1–9). <https://doi.org/10.1145/3206343.3206349>
- [9] Pășărică, A., Bozomitu, R. G., Cehan, V., Lupu, R. G., & Rotariu, C. (2015, October). Pupil detection algorithms for eye tracking applications. *2015 IEEE 21st International Symposium for Design and Technology in Electronic Packaging (SIITME)* (pp. 161–164). IEEE. <https://doi.org/10.1109/SIITME.2015.7342317>
- [10] Stengel, M., Grogorick, S., Eisemann, M., Eisemann, E., & Magnor, M. A. (2015, October). An affordable solution for binocular eye tracking and calibration in head-mounted displays. *Proceedings of the 23rd ACM international conference on Multimedia* (pp. 15–24). <https://doi.org/10.1145/2733373.2806265>
- [11] Wen, Q., Bradley, D., Beeler, T., Park, S., Hilliges, O., Yong, J., & Xu, F. (2020). Accurate Real-time 3D Gaze Tracking Using a Lightweight Eyeball Calibration. *Computer Graphics Forum*, 39(2), 475–485. <https://doi.org/10.1111/cgf.13945>
- [12] Lee, G. J., Jang, S. W., & Kim, G. Y. (2020). Pupil detection and gaze tracking using a deformable template. *Multimedia Tools and Applications*, 79(19), 12939–12958. <https://doi.org/10.1007/s11042-020-08638-7>
- [13] Gegenfurtner, A., Lehtinen, E., & Säljö, R. (2011). Expertise differences in the comprehension of visualizations: A meta-analysis of eye-tracking research in professional domains. *Educational Psychology Review*, 23(4), 523–552. <https://doi.org/10.1007/s10648-011-9174-7>
- [14] Sarkar, N., O’Hanlon, B., Rohani, A., Strathearn, D., Lee, G., Olfat, M., & Mansour, R. R. (2017, January). A resonant eye-tracking microsystem for velocity estimation of saccades and foveated rendering. *IEEE 30th International Conference on Micro Electro Mechanical Systems (MEMS)* (pp. 304–307). IEEE. <https://doi.org/10.1109/MEMSYS.2017.7863402>
- [15] Bartuzel, M. M., Wróbel, K., Tamborski, S., Meina, M., Nowakowski, M., Dalasiński, K., Szkulmowska, A. & Szkulmowski, M. (2020). High-resolution, ultrafast, wide-field retinal eye-tracking for enhanced quantification of fixational and saccadic motion. *Biomedical Optics Express*, 11(6), 3164–3180. <https://doi.org/10.1364/BOE.392849>
- [16] Meyer, J., Schlebusch, T., Fuhl, W., & Kasneci, E. (2020). A novel camera-free eye tracking sensor for augmented reality based on laser scanning. *IEEE Sensors Journal*, 20(24), 15204–15212. <https://doi.org/10.1109/JSEN.2020.3011985>
- [17] Pomianek, M., Piszczek, M., Maciejewski, M., & Krukowski, P. (2020, October). Pupil Position Estimation Error in an Eye Tracking System Based on the MEMS Mirror Scanning Method. *Proceedings of the 3rd International Conference on Microelectronic Devices and Technologies (MicDAT’ 2020)* (pp. 28–30). IFSA.
- [18] Pengfei, Y., Zhengming, C., Jing, T., & Lina, Q. (2016). Virtual Simulation System of Cutter Suction Dredger Based on Unity3D. *Journal of Systems Simulation*, 28(9), 2069–2075.
- [19] Richards, D., & Taylor, M. (2015). A Comparison of learning gains when using a 2D simulation tool versus a 3D virtual world: An experiment to find the right representation involving the Marginal Value Theorem. *Computers & Education*, 86, 157–171. <https://doi.org/10.1016/j.compedu.2015.03.009>
- [20] Müller, L. M., Mandon, K., Gliesche, P., Weiß, S., & Heuten, W. (2020, November). Visualization of Eye Tracking Data in Unity3D. *19th International Conference on Mobile and Ubiquitous Multimedia* (pp. 343–344). <https://doi.org/10.1145/3428361.3431194>



Mateusz Pomianek received the B.Sc. degree in Mechatronics in 2016 and the M.Sc. degree in Optoelectronics in 2017, both from the Military University of Technology (MUT). He is currently pursuing the Ph.D. degree in the field of Automatics, Electronics and Electrical Engineering. His research activity focuses on optoelectronic technologies in virtual reality systems, eye tracking and natural user interfaces.



Marek Piszczek received the Ph.D. degree from Military University of Technology, Poland, in 2000. He is currently Assistant Professor at the same university. He has authored or co-authored 6 monograph, 90 articles, and 3 patent applications. His current research interests include engineering of image information in research and application, active imaging, machine vision, virtual and augmented reality.



Marcin Maciejewski obtained the B.Sc. and M.Sc. degrees in Electronics from the Military University of Technology (MUT), Warsaw, Poland in 2014 and 2015, respectively. He is currently pursuing the Ph.D. degree in the field of Automatics, Electronics and Electrical Engineering. His current research interests include optoelectronic, technologies in virtual reality, especially in the field of motion capture systems.